Atmos. Chem. Phys., 10, 6669–6684, 2010
www.atmos-chem-phys.net/10/6669/2010/
doi:10.5194/acp-10-6669-2010

Atmospheric Chemistry and Physics

Vertical transport rates and concentrations of OH and Cl radicals in the Tropical Tropopause Layer from observations of CO_2 and halocarbons: implications for distributions of long- and short-lived chemical species

S. Park[1], E. L. Atlas[2], R. Jiménez[1], B. C. Daube[1], E. W. Gottlieb[1], J. Nan[1], D. B. A.Jones[3], L. Pfister[4], T. J. Conway[5], T. P. Bui[4], R.-S. Gao[5], and S. C. Wofsy[1]

[1]Dept. of Earth and Planetary Sciences and the School of Engineering and Applied Sciences, Harvard University, Cambridge, MA, USA
[2]University of Miami, Rosenstiel School of Marine and Atmospheric Science, Miami, FL, USA
[3]Dept. of Physics, University of Toronto, Toronto, Ontario, Canada
[4]NASA, Ames Research Center, Moffett Field, CA, USA
[5]NOAA, Earth System Research Laboratory, Boulder, CO, USA

Received: 22 February 2010 – Published in Atmos. Chem. Phys. Discuss.: 1 March 2010
Revised: 26 May 2010 – Accepted: 8 July 2010 – Published: 21 July 2010

Abstract. Rates for large-scale vertical transport of air in the Tropical Tropopause Layer (TTL) were determined using high-resolution, in situ observations of CO_2 concentrations in the tropical upper troposphere and lower stratosphere during the NASA Tropical Composition, Cloud and Climate Coupling (TC4) campaign in August 2007. Upward movement of trace gases in the deep tropics was notably slower in TC4 than during the Costa Rica AURA Validation Experiment (CR-AVE), in January 2006. Transport rates in the TTL were combined with in situ measurements of chlorinated and brominated organic compounds from whole air samples to determine chemical loss rates for reactive chemical species, providing empirical vertical profiles for 24-h mean concentrations of hydroxyl radicals (OH) and chlorine atoms in the TTL. The analysis shows that important short-lived species such as $CHCl_3$, CH_2Cl_2, and CH_2Br_2 have longer chemical lifetimes than the time for transit of the TTL, implying that these species, which are not included in most models, could readily reach the stratosphere and make significant contributions of chlorine and/or bromine to stratospheric loading.

Correspondence to: S. C. Wofsy
(swofsy@seas.harvard.edu)

1 Introduction

Inputs of trace gases into the stratosphere are controlled by transport processes and chemistry in the Tropical Tropopause Layer (TTL). Most stratospheric radicals are derived from the breakdown of tropospheric source gases including a wide variety of natural and anthropogenic halocarbons, N_2O, and CH_4. The efficiency with which a tropospheric source gas is transported through the TTL into the stratosphere depends on the relative rates for chemical removal versus the time required to transit the TTL. Source gases from the lower troposphere are detrained into the TTL in the outflow from deep convective storms; if subsequent transport to the stratosphere in the TTL is sufficiently rapid these compounds will enter the stratosphere where they break down and add to the burden of lower stratospheric bromine, chlorine, etc. But if these species react within the TTL, the inorganic products are subject to scavenging by clouds (e.g., convective anvils and subvisual cirrus) or aerosols, and the associated halogen atoms may never reach the stratosphere.

In this paper, we use detailed measurements of trace gases in the TTL with a wide range of chemical lifetimes, from a few days to infinite (nonreactive), to empirically constrain both the chemical lifetimes and the transport time scales for key species, emphasizing the precursors of stratospheric inorganic halogens. The observations were carried

out over Costa Rica and adjacent ocean areas using the NASA WB-57F high-altitude aircraft during the Tropical Composition, Cloud and Climate Coupling (TC4) campaign in August 2007 (Toon et al., 2010). Results from TC4 are compared to similar observations made during the Costa Rica AURA Validation Experiment (CR-AVE) in January 2006.

We first use high-resolution in situ observations of CO_2 to constrain the age spectrum and associated vertical transport rates and residence times for air in the TTL, as we have done previously for the lower stratosphere (Andrews et al., 1999; Andrews et al., 2001a, b; Boering et al., 1996). In the wintertime TTL, during CR-AVE, air was advected upward rapidly, and the seasonal variation of CO_2 allowed us to define a CO_2 *tracer clock* (Park et al., 2007). For TC4, due to the slower rates of vertical advection, we use a one-dimensional (1-D) advection-diffusion transport approach equivalent to the age spectrum concept of Hall and Waugh (1997, 2000; e.g., Gettelman et al., 2009), and we apply this result to CR-AVE data as well.

Next we use the transport properties of the TTL obtained from CO_2 to evaluate observations of reactive species, in order to infer rates of photochemical removal and to understand the efficiency with which these tracers propagate into the stratosphere via large-scale ascent of air mass in the TTL versus other possible pathways. The Whole Air Sampler on the WB-57F (WAS; see Sect. 2 for instrumental details) (Flocke et al., 1999; Schauffler et al., 1999, 2003) provided a comprehensive suite of measurements of chlorinated and brominated organic compounds, non-methane hydrocarbons and alkyl nitrates. We analyze data for selected gases representing a wide range of photochemical lifetimes in the TTL. Most of these species are removed primarily by photolysis and reaction with hydroxyl radical (OH), allowing us to deduce empirically the 24-h mean OH vertical distribution in the TTL from an optimal fit of the photochemical transport simulation to the observations. A few short-lived species have significant loss rates due to reactions with chlorine (Cl) atoms, e.g., ethane (C_2H_6) and tetrachloroethene (C_2Cl_4), allowing us to empirically determine atomic chlorine concentrations as well, although the constraints are somewhat weaker. The OH radical and Cl atom concentrations derived here can be used to determine the lifetimes of a wide range of chemicals in the TTL and as a check on photochemical models. Concentrations of OH calculated from photochemical models may be underestimated, due mainly to failure in simulating high concentrations of OH near sunrise and sunset (e.g., Salawitch et al., 1994; Wennberg et al., 1998), leading to uncertainties in the model predictions of the amounts and distributions of organic and inorganic halogenated compounds.

Information on the measurements is provided in Sect. 2. The conceptual framework used in our analysis is described in Sect. 3. In Sect. 4, we present the simulation results and discuss the derived vertical profiles for air transport rates and reactive agents. The implications of the estimates of local lifetime for major long- and short-lived halogenated compounds are also considered. Conclusions follow in Sect. 5.

2 Measurements

Measurements of CO_2 mixing ratios on the NASA WB-57F aircraft were made using a nondispersive infrared absorption analyzer flown in many previous experiments (see Daube et al., 2002 for details). The instrument was calibrated every ∼10 min in flight, with demonstrated long-term precision of 0.1 ppmv (Boering et al., 1995). Flight standards were calibrated against CO_2 world standards from the National Oceanic and Atmospheric Administration/Earth System Research Laboratory (NOAA/ESRL), and thus are directly comparable to surface data from the ESRL global network, with accuracy better than 0.2 ppmv.

Air samples were collected with the Whole Air Sampler (WAS) (Flocke et al., 1999; Schauffler et al., 1999, 2003), consisting of 28 to 40 1.6-l electropolished stainless steel canisters, a 4-stage metal bellows pump, a stainless steel manifold, motor-driven valves, and an electronics package for valve and pump control. The metal bellows pump pressurized the instrument manifold to 40 psia (2.7 bar), resulting in a sample volume of ∼4.5 standard liters (STP). The filling time varied between 15 and 180s, depending on flight altitude. Filled canisters were transported to University of Miami for analysis. Mixing ratios of approximately 50 different species were measured, including CFCs, HCFCs, HFCs, halons, other halogenated compounds, and alkyl nitrates on the WAS samples by gas chromatography with mass selective detection (GC-MS) (Hewlett Packard models 5890 and 5971) using electron impact ionization. Calibrations were based on in-house prepared standards and on commercial halocarbon mixtures that were calibrated using gas chromatography with atomic emission detection (GC/AED) versus various NIST standards or standards referenced to NIST mixtures. The detection limits and measurement accuracy varied due to different individual responses and background noise, but are generally better than 0.1 pptv and 15%, respectively.

A large number of other tracer and meteorological measurements were made on the aircraft, providing important information on the chemical and dynamical context of the sampled air. Air temperature and pressure were measured by the Meteorological Measurement System (MMS) on board the aircraft, with precision and accuracy of ±0.1 K and ±0.3 K, respectively, for temperature, and ±0.1 hPa and ±0.3 hPa, for pressure (Scott et al., 1990). These parameters were used to derive potential temperate with an uncertainty of ∼2 K. In situ ozone measurements were made by the NOAA Dual-Beam UV Absorption Ozone Photometer (Proffitt and McLaughlin, 1983). At a 1-s data collection rate, measurement precision is ±0.6 ppbv (STP) and average uncertainty is ∼±5%.

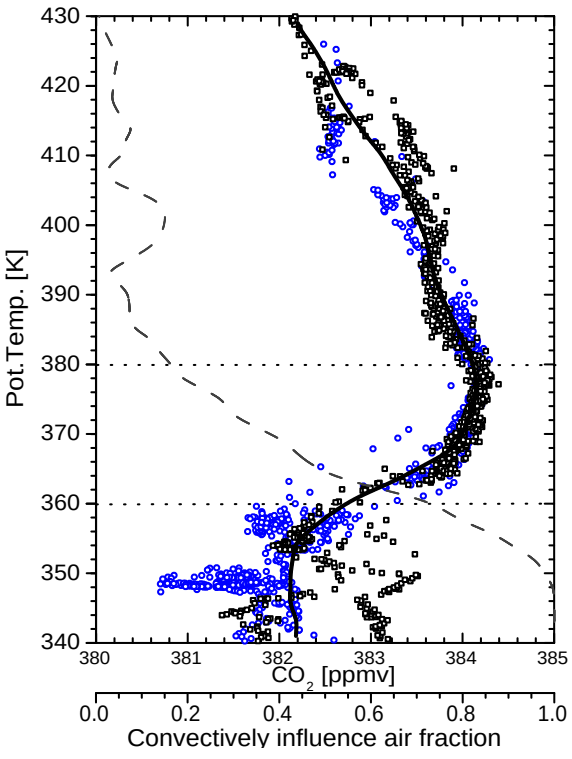

Fig. 1. Vertical profiles of CO_2 from two science flights in the tropics (<11° N) on 5 (denoted by blue empty circles) and 6 August(by black empty squares) during TC4. The line is a fit (locally-weighted least squares, "lowess") to averages in 1-K intervals of potential temperature. Fraction of air cluster points with non-zero convective influence, which was calculated by back trajectory analyses to convective systems, based on the method of Pfister et al. (2001, 2010). The dashed line shows the 1-K averaged fraction of air clusters influenced by convection for 14 day trajectories, which is concentrated mainly below the TTL, reducing to low values above 360 K. For the higher levels (near 400 K), the occasional impact of convection seems to appear in the convective influence fraction and short lived species, but not in the CO_2 profile. Two horizontal dotted lines denote the bottom of the TTL and cold point temperature altitude.

3 Analysis

3.1 CO_2 of the TTL in NH summer

There are a number of definitions of the TTL in the literature. Here we consider the top of the TTL to be the tropopause, defined as the level of the cold point at ∼17–19 km (near ∼380 K) (Gettelman and Forster, 2002), and the bottom to be the level below which we observe a sharp increase in both the variance of the CO_2 concentration and in the Fraction of Convectively Influenced air mass computed from diabatic trajectories mapped onto satellite data for convective cloud tops (see Fig. 1; refer to Pfister et al., 2001, 2010, and Park et al., 2007 for details). The dynamical and chemical properties of the atmosphere (e.g., upward mass flux; temperature lapse rate; the balance between convection and slow radiatively driven ascent; the mixing ratios of ozone, water vapor and other chemical tracers) change from tropospheric at the base of the TTL to stratospheric at the top.

During TC4, the influence of convection subsided noticeably above the ∼360-K level, as indicated by the sharp reduction both in the variance of the CO_2 concentration and in the computed Fraction of Convectively Influenced air. Thus, we set the base of the TTL at $\theta = 360$ K (∼14.8 km altitude), somewhat above the lower bound of the TTL recently defined by Fueglistaler et al. (2009) (355 K, ∼150 hPa, 14 km), but similar to their determination of the level of zero radiative heating under clear-sky conditions.

Park et al. (2007) analyzed the wintertime TTL observed in the CR-AVE mission in 2006. They found that the CO_2 seasonal trend at the surface (CO_2 increasing with time) is preserved in a compact form throughout the TTL above 360 K, indicating that air in this region aged monotonically with altitude with near-zero age at 360K. A simple "CO_2 tracer clock" can be defined during this season that gives a good constraint on TTL ascent rates and a good approximation to the mean age. The seasonal curve in January has no extremum, making it difficult to determine dispersion rates and a full age spectrum using CO_2 data from CR-AVE.

However, the CO_2 clock is inapplicable in August, during TC4, because the seasonal maximum in May–June makes the CO_2 profile non-monotonic in TC4 (Fig. 1) (cf. Boering et al., 1994), and, as we shall see, the vertical transport times are slower. Nevertheless the seasonal cycle at the surface is faithfully traced out in the vertical dimension within the TTL, with its amplitude attenuated. We approach this problem by solving for the full age spectrum using the one-dimensional advection-diffusion equation, as envisioned by Hall and Waugh (2000) and described in detail in Sect. 3.2. The observed monotonic progression of mean age implies that the ensemble mean transport of trace gases can be assessed using a simple one-dimensional column approach, even though atmospheric motions are complex and 3-dimensional (Hall and Waugh, 2000; Gettelman et al., 2009); clearly, though, this simplified approach has limitations.

Data from TC4 tropical flights are best presented in potential temperature coordinates (Fig. 1), in order to remove the variance associated with reversible adiabatic displacements of the atmosphere. However, when we analyze reactive species we must use height as the vertical coordinate since the photochemical properties of the atmosphere (e.g., reaction rate coefficients with OH radical, photolysis rate constants, etc) are functions of altitude and pressure, not potential temperature. Hence in this paper we use mean tracer concentrations versus altitude for the analysis of rates of transport and chemistry in TC4 (e.g., see Fig. 3a for CO_2; note the artificial variability introduced by using altitude instead of potential temperature as the independent variable).

The latitude range selected as "tropics" was 2° N to 10° N, limited on the southern end by the range of the WB-57F. We

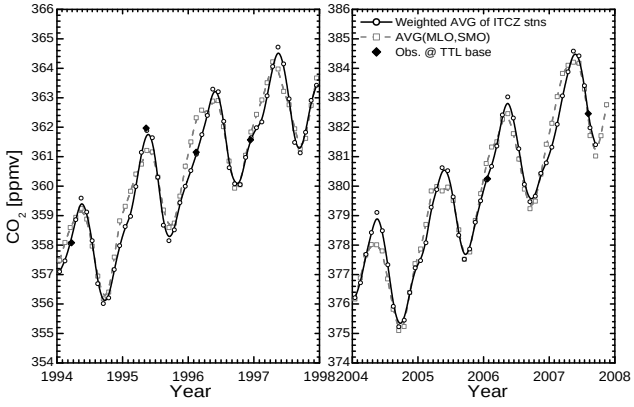

Fig. 2. Boundary condition for CO_2 entering the TTL. Solid curve is the weighted average of surface data from NOAA ESRL stations located in the ITCZ (Conway et al., 1994). The previous CO_2 index defined as average data for CO_2 at Mauna Loa (MLO) and Samoa (SMO) is plotted as gray dashed curve. Filled diamonds represent data obtained near 360 K (∼15 km) during ASHOE, STRAT, CRAVE, and TC4: Airborne Southern Hemisphere Experiment (ASHOE) from March to November 1994; Stratospheric Tracers of Atmospheric Transport (STRAT) from May 1995, October to November 1995, January to February 1996, July to August 1996, September 1996, December 1996; CR-AVE in January to February 2006; TC4 in August 2007.

noted however that the 8 August CO_2 profile was clearly very different from the other two days. There is evidence that the air on the vertical descent profile on this day was influenced by very deep convection over Lake Maracaibo upstream of the point of observation, as shown by trajectory calculations using the method of Pfister et al. (2010). This convective influence extended well above the cold point tropopause. Observations of such convection may provide insight into the mechanism of rapid direct injection of boundary layer air to the upper part of the TTL, but they were excluded from our analysis in order to focus on the integrated mean distribution of transit times that characterize the bulk of the observations.

We derived a CO_2 index to describe zero-age air entering the TTL using the seasonally varying weighted average of ground data from stations within the ITCZ (represented by solid lines in Fig. 2). All stations within the seasonal varying ITCZ were considered and the weight of a station at a given time is determined by the station's position relative to the ITCZ at that time. The resulting values correspond more closely to observed CO_2 mixing ratios at the base of the TTL from tropical aircraft missions spanning more than 12 years, as shown in Fig. 2. This index represents an improvement from the monthly average of concentration data for CO_2 at Mauna Loa (MLO, 19° N) and Samoa (SMO, 14° S) (Fig. 2; denoted by gray dashed lines) used by Boering et al. (1996) and Park et al. (2007), as needed to describe the small age differences observed within the TTL.

3.2 One-Dimensional advection-diffusion model

The equation for our 1-D column model describes mass continuity of tracer with mole fraction c in a column,

$$\underset{\text{I}}{\frac{\partial c}{\partial t}N} - \underset{\text{II}}{\frac{\partial}{\partial z}K_Z N\frac{\partial c}{\partial z}} + \underset{\text{III}}{wN\frac{\partial c}{\partial z}} + \underset{\text{IV}}{N\alpha f\frac{c-c_o}{\tau_{\text{conv}}}} = \underset{\text{V}}{P-L} \qquad (1)$$

where N is the number density (m^{-3}) of the atmosphere at height z; $N(z) = N_0 e^{-z/H}$ and H is the scale height ($H = 5808$ m for TC4), w is the ascent rate in $m\,s^{-1}$, K_z is the effective diffusion coefficient along the vertical direction in $m^2\,s^{-1}$, f is the fraction of air injected by deep convection over time scale τ_{conv} (Gettelman et al., 2009), α is the efficiency of convective transport, and $P-L$ is the net photochemical rate ($m^{-3}\,s^{-1}$; = 0 for CO_2; $= -k_c N$ for reactive species, k_c is the loss frequency). Convective injection (term IV) is included for completeness. The influence of term IV cannot be distinguished from vertical advection (see discussion below) in TC4 or CR-AVE.

The domain extends from $z = 14.8$ km (equivalent to ∼360 K) to $z = 25$ km, which is given zero flux for CO_2. Time zero (t_0) was set to be two years prior to the observation, since the air in the TTL and lower tropical stratosphere turns over on timescales of months. The initial CO_2 profile at t_0 was represented by subtracting from the profile observed during TC4 (i.e., Fig. 3) the CO_2 concentration difference between the modified CO_2 index at t_0 and the CO_2 index at the mission time. The lower spatial boundary (i.e., $z = 14.8$ km) corresponds to zero age, with CO_2 given by the modified CO_2 index (see Sect. 3.1). The final time point in the integration of term I gives the derived profile at the mission time. The time step is 0.5 days and the z interval is 50 m, to create a high-resolution profile. We represent w as an unknown exponential function with altitude, $w = a_0 \times \exp[-(z - z_0)/(b_0 \times H)]$ with a_0 and b_0 as inputs to be adjusted. K is assumed an unknown constant with height, since there is only one seasonal extremum which characterizes K on average through the TTL. Results are similar if a simple quadratic polynomial is used to represent w. The model-generated profile can then be compared to in situ CO_2 measurements to determine the optimal representation of the w and K functions by minimizing the root mean square error (RMSE), with the additional constraint that there be a close match to the altitude of the CO_2 seasonal maximum. The age spectrum for the TTL is derived by superposition of the solutions to the 1-D equation with unit input, using the optimized coefficients w and K (Hall and Waugh, 2001).

Twenty-four-hour mean photolysis rate constants (J) for the selected tracers were calculated as functions of altitude using the Harvard two-dimensional model (Schneider et al., 2000), with temperature dependent absorption cross sections from Sander et al. (2006). The radiation field is calculated

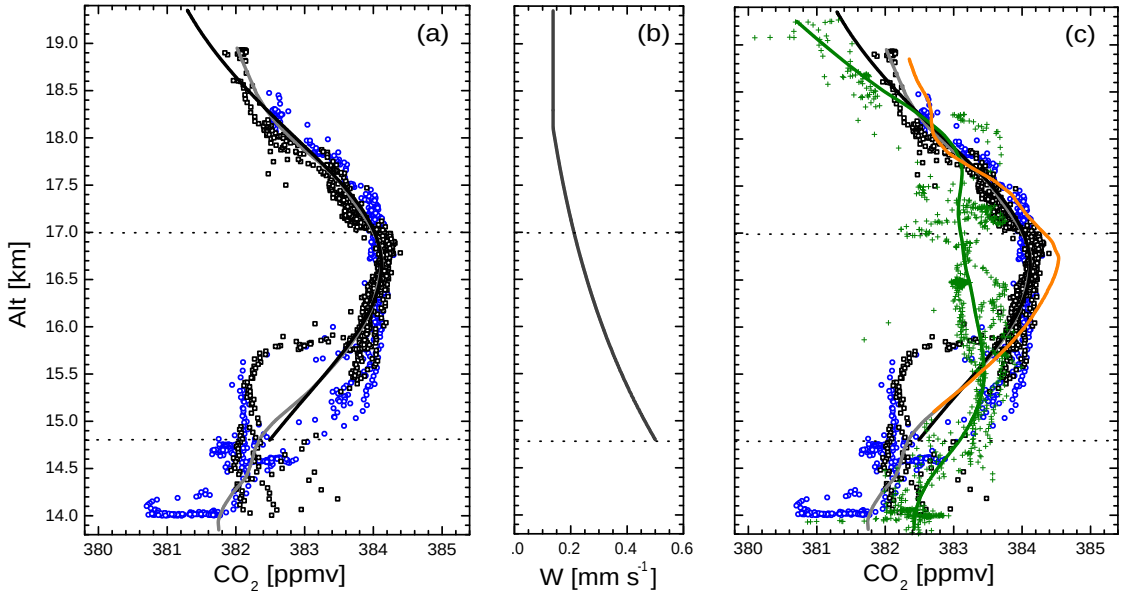

Fig. 3. **(a)** Vertical profiles of CO_2 obtained on 5 and 6 August . All values are same as shown in Fig. 1, but are plotted against altitude. The gray line denotes the smoothed CO_2 profiles. The black solid line corresponds to the best fit to the observations with the optimum $w(z)$ and K. The lack of compactness found in the altitude profile between 14.7 km and 16 km unlike the θ–space profile in Fig. 1 is due to vertical, reversible fluctuation of air particles. **(b)** Vertical profile of ascent rate, $w(z)$ derived from the 1-D advection-diffusion model. **(c)** Observations between 25° N and 35° N for two transit flights on 3 and 9 August are plotted with green cross symbols. When assuming that the observed profile in Fig. 3a is a result of dilution by horizontal mixing along the isentropic levels and 30% of air mass in the profile is originated from the extratropics, the hypothetical CO_2 profile before the dilution is given in the orange line. Note the maximum of the profile corresponds to the seasonal peak (384.5 ppmv CO_2) of the modified CO_2 index that occurred in May 2007.

using a six-stream approximation for clear-sky conditions assuming a multiple scattering atmosphere and representative albedo for the underlying atmosphere and surface. Temperatures from TC4 were used in the calculation of photolysis cross sections. Ozone profiles, needed for the full height range above the measurement region, were based on the results of Parrington et al. (2008) for August 2006, obtained through assimilation of ozone observations from the Tropospheric Emission Spectrometer (TES) into the GEOS-Chem model for 100 hPa and below. Above 100 hPa the ozone field was determined by linearized stratospheric ozone chemistry (McLinden et al., 2000) in GEOS-Chem.

The loss frequencies for oxidation were derived from the reaction rate constants given by Sander et al. (2006) multiplied by [OH] profiles adjusted from the base profiles calculated by both the Global Modeling Initiative (GMI) model (Considine et al., 2008) for July 2007 and the Geos-Chem model (Wang et al., 2008) for August 2003. The scaling function for OH was defined as a 2nd-order polynomial function with altitude and adjusted to optimize agreement with measured tracer profiles, solving Eq. (1) numerically. We considered 9 short- and long-lived tracers, selected to be representative of the primary organic source gases of chlorine and bromine to the upper troposphere and lower stratosphere, with a broad range of lifetimes from a few weeks to several years: CFC-11 (CCl_3F), Halon-2402 ($CBrF_2CBrF_2$), carbon tetrachloride (CCl_4), methyl chloroform (CH_3CCl_3), methyl chloride (CH_3Cl), methyl bromide (CH_3Br), chloroform ($CHCl_3$), dibromomethane (CH_2Br_2), and bromoform ($CHBr_3$). The lower boundary condition for the mixing ratio of each species was determined as the mean of observations at isentrope 360-K (∼14.7–14.8 km). The upper boundary condition was an extrapolated flux (=LH, where L is the loss rate ($m^{-3}\,s^{-1}$) at 25 km).

Reaction with chlorine (Cl) atoms is a dominant sink for some short-lived species in the TTL and lower stratosphere, e.g., ethane (C_2H_6) and tetrachloroethene (C_2Cl_4). We estimated the vertically averaged 24-hr mean Cl concentration by estimating the required Cl loss rate to account for the difference between the observed profiles for C_2H_6 and C_2Cl_4 and its modeled fit using the optimum OH from the other species. Since these species are all short-lived, there were too few tracer data points dependent on Cl to allow us to derive a profile for Cl.

4 Results and discussion

4.1 CO_2 and vertical transport properties

The CO_2 data obtained on 5 and 6 August were binned to 50-m altitude and the mean for each altitude bin was calculated. The means were then smoothed using locally weighted least squares ("lowess", smoothing window 0.075) to give representative profiles for the TTL. The optimized profile of w was $5\times10^{-4}\exp[-(z-z_0)/(0.44\times H)]\,\mathrm{m\,s^{-1}}$ between the bottom of the TTL (i.e., z_0=14.8 km) and the cold point ($\sim$17 km), corresponding to 0.50 mm s^{-1} and 0.20 mm s^{-1} at the lower and upper boundaries, respectively. Above 18 km altitude, w of 0.14 mm s^{-1} was found to accomplish the best fit (Fig. 3b). The average in the TTL and the lower stratosphere (14.7–19 km) was $w = 0.25\pm0.11$ mm s^{-1} and K was 0.063 m^2 s^{-1} throughout the profile. The resulting RMSE between the generated profile and the empirical observations is only 0.08 ppmv. Using other functional forms for w gives similar results; the mean value and decrease with altitude by a factor of 2–3 are robust.

It is notable that the ascent rate *decreases* with altitude, implying detrainment of most of the upwelling air into the extratropics (if there were no detrainment, w would increase exponentially as $N(z)^{-1}$). This result is consistent with recent findings from trajectory analysis (Levine et al., 2007) that quasi-isentropic transport into the extratropical lowermost stratosphere is significant. The TTL age spectrum derived from the advection-diffusion equation is consistent with the results for the lower tropical troposphere presented by Andrews et al. (1999). The results are also consistent with the analysis of satellite data by Gettelman et al. (2009), although these authors attribute much of the vertical transport in the lower TTL to convective influence (see discussion below).

We tested this 1-D advection-diffusion model framework for the CO_2 data obtained in the boreal winter during the CR-AVE. The observations on 21 and 22 January were selected, representing the middle of the mission period with relatively frequent WAS samples. We obtained a best-fit of $w = 1.1\times10^{-3}\ \exp[-(z-z_0)/(4\times H)]\,\mathrm{m\,s^{-1}}$ between 13.5 km and 17.6 km (i.e., near the cold point) and above the altitudes, $w = 0.9\times10^{-3}\ \exp[-(z-z_0)/(0.085\times H)]\,\mathrm{m\,s^{-1}}$ throughout the lower stratosphere, which correspond to 1.1 mm s^{-1} and 0.4 mm s^{-1} at the bottom of the TTL and at 18 km, respectively. The vertical diffusion coefficient K for an optimal fit was 0.1 m^2 s^{-1} but it was not well constrained due to the linear character of the CO_2 profile. The RMSE of the best fit was also quite small, only 0.07 ppmv. These estimates of vertical diffusion coefficients for summer and winter are compatible to the values in the range of 0.03 and 0.1 m^2 s^{-1}, proposed for the tropical lower stratosphere by Andrews et al. (1999).

The calculated vertical ascent velocity w in the TTL in winter is smaller if K is included compared to the estimate using the tracer clock, which combines transport from advection and from non-conservative dispersion. The winter time vertical velocity was much larger than the summer velocity at the same level. When our altitude-varying w's for winter are averaged throughout the altitude range of 13.5 km and 19 km, we obtain 0.8 ± 0.3 mm s^{-1}, comparable to the value estimated by Schoeberl et al. (2008) for CR-AVE. These authors re-analyzed the same CO_2 data set from the CR-AVE to constrain an ascent rate with the following modification: (1) Since the variability at 360 K is too large to derive statistically significant time-varying trend, the data only from 370 K to 390 K were considered. (2) The altitude gradient (ΔCO_2) between 370 K and 390 K was coupled with the actually observed trend at 370 K during the mission period of 24 days, instead of the trend from the CO_2 index. (3) Therefore, they introduce larger uncertainties from the observed gradient and the observed time trend into the calculation. Then they computed the ascent rate of 0.6 ± 0.3 mm s^{-1} in the altitudes of 16.0–17.8 km and suggested that the apparent ascent rate can be estimated down to corrected value of $\sim$0.3 mm s^{-1}, accounting for both vertical and horizontal eddy diffusion terms, which they argued contributes nearly half of the transport. Interestingly, more recent model calculation using diabetic heating rates (Kruger et al., 2009) suggested 70 days of mean residence time of air mass for θ = 360–400 K layer in the TTL and a back trajectory analysis (Ploeger et al., 2010), which was performed to test various vertical velocity scenarios used in transport models, showed that annual mean vertical velocity is in the range of 0.6 K day^{-1} and 1.2 K day^{-1}. These results correspond to ascent rate of 0.7 mm s^{-1} to 1.4 mm s^{-1} in large-scale vertical transport, compatible to or slightly higher than our estimate.

Note a rigorous estimate of the uncertainty in our values of w and K is difficult to obtain because several non-statistical uncertainties are linked together (e.g., imperfect knowledge of the CO_2 boundary condition). It's especially difficult to accurately quantify the error associated with our assumption that transport in the TTL and lower stratosphere can be adequately represented using the 1-D advection diffusion equation without accounting for quasi-horizontal mixing between the tropics and extratropics, the major process invoked by Schoeberl et al. (2008). We note that the observed compact structure of both CO_2 and O_3 profiles (not shown here) indicates that the effect of midlatitude air entrainment is relatively small.

The error analysis in the apparent ascent and diffusion rates related with horizontal mixing is limited due to lack of information to specify a representative profile of CO_2 in the extratropics and the amount of air entering from the extratropics. In order to investigate how much mixing of older extratropical air into the tropics might alter CO_2 profiles and thus change the values of w and K, we assumed that the observations between 25° N and 35° N for two transit flights on 3 and 9 August were representative of extratropical CO_2 (green symbols and line in Fig. 3c). If we further assume

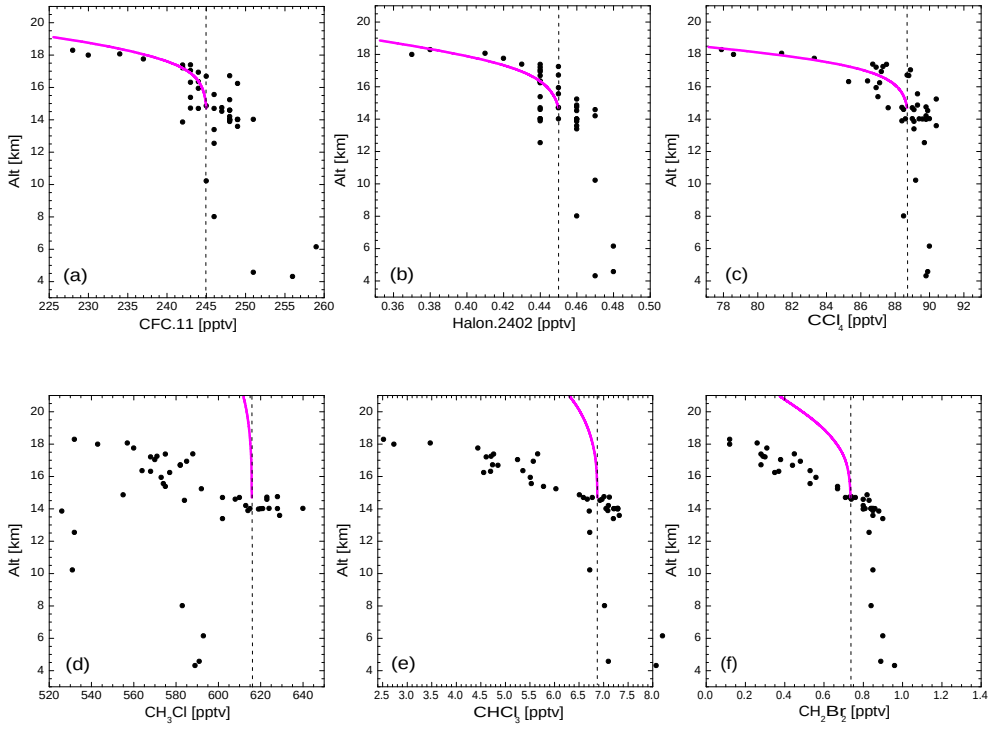

Fig. 4. Vertical distributions of **(a)** CFC-11, **(b)** Halon-2402, **(c)** CCl_4, **(d)** CH_3Cl, **(e)** $CHCl_3$, and **(f)** CH_2Br_2. Plotted are individual data points (solid circles) measured by WAS on 5 August and the 1-D model results using photolysis rates alone as photochemical input (pink solid lines). Note that all calculations are based on the transport rates determined by CO_2.

that the maximum of a tropical profile in the absence of isentropic exchange cannot be larger than the seasonal peak (384.5 ppmv CO_2) of the modified CO_2 index (see Fig. 2) in May 2007, the percentage of air in the TTL that originated from the extratropical stratosphere cannot be more than ∼30%. The hypothetical CO_2 profile before 30% dilution by the extratropical CO_2 is shown in Fig. 3c (orange line), for which the ascent rate would be $0.24\pm0.10\,\mathrm{mm\,s^{-1}}$ on average and statistically same as the rate derived from our model analysis. The vertical diffusion coefficient would be significantly reduced, to $0.008\,\mathrm{m^2\,s^{-1}}$, the horizontal exchange carries on the role of vertical eddy diffusion. These w and K values will also be tested with the WAS species below.

We also investigated the inclusion of term IV in Eq. (1), representing direct injection by deep convection that penetrates to the TTL in a profile that dies off rather rapidly above 360K (Fig. 1; cf. Gettelman et al., 2009). We assumed that f was given by the fraction of air affected by convection (Fig. 1) over the trajectory time scale (τ_{conv} = 14 days). With α= 1, the air was too young below 365 K, the lowest part of the TTL, and there was no way the model could fit the data. There were not sufficient constraints from CO_2 data to optimize α (<1) along with w and K in this region. Thus the effects of 1-D advection-diffusion and convective influence on CO_2 are indistinguishable in the lowest part of the TTL. The influence of convection was very small above 370 K, comprising the upper half of the TTL. This result is confirmed by our analysis of reactive species (see below).

The effective equivalence between the 1-D advection-diffusion approach and more detailed models that incorporate convective inputs and/or isentropic exchange reflect the fundamental characteristic of the CO_2 profiles observed in the TTL in both TC4 and CR-AVE: in both seasons, the observed profiles are only moderately modified from the time history obtained using the CO_2 index in the tropics. This basic characteristic implies that air in the TTL ages monotonically, covering a period of weeks from bottom to top, and also that the age spectrum is relatively sharply peaked. The measurements do not reveal exactly how atmospheric motions create the age spectrum; e.g., there might be a small mode representing older air from mid latitudes that is missing from our formulation. But these details are not essential to simulate the major features of net vertical transport of CO_2 or other tracers that originate near the surface in the ITCZ.

4.2 Photochemistry for long- and short-lived species

The vertical distributions of in situ measurements obtained on 5 August are presented in Figs. 4 and 5. We focus on 6 chemical species first: CFC-11, Halon-2402, CCl_4, CH_3Cl, $CHCl_3$, and CH_2Br_2 in Fig. 4a–f (denoted by black filled circles). The mixing ratios of CFC-11, Halon-2402, and CCl_4

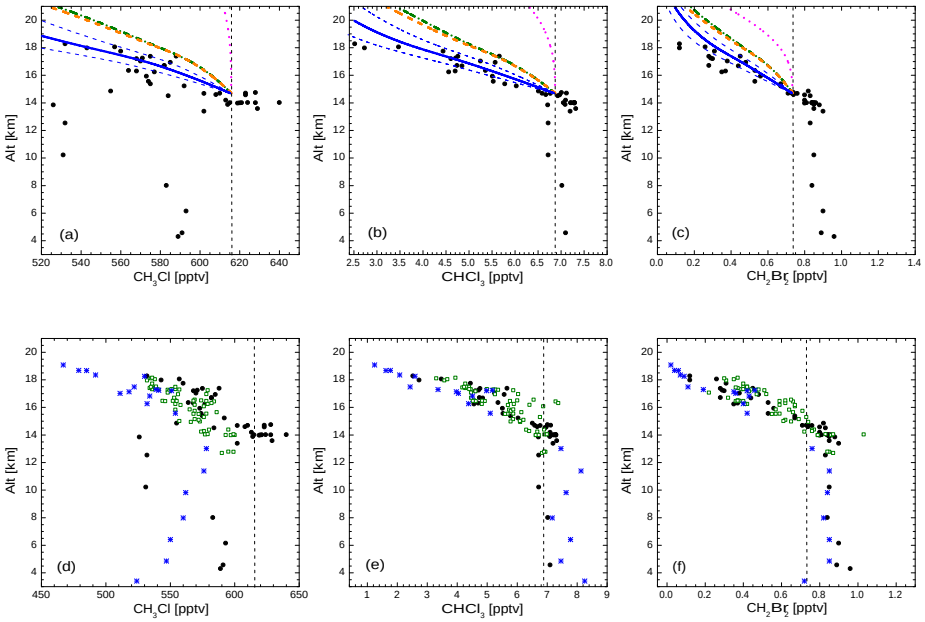

Fig. 5. Vertical distributions of **(a)** CH_3Cl, **(b)** $CHCl_3$, and **(c)** CH_2Br_2. Shown are the simulated profiles of 1-D model using combined inputs of photolysis and reaction with OH radicals. Dash-dotted green lines represent the base case using the OH estimate derived from the GMI model. The dashed orange lines denote the resulting simulation with the GMI-derived OH estimate, and the w and K values determined from the hypothetical profile (orange line in Fig. 3c). An adjusted OH profile with a scaling term of 2nd polynomial function from the base OH give the best fits to the all three observations. The simulation results using the optimal OH concentration profile are shown in blue solid lines. The blue dashed lines around the solid one correspond to uncertainties in the simulation that ±30% uncertainties in [OH] (blue dotted lines in Fig. 6) can produce. Photolysis-only runs are plotted as pink dotted lines. Vertical profiles of **(d)** CH_3Cl, **(e)** $CHCl_3$, and **(f)** CH_2Br_2 in the TTL (<11° N) are compared with observations both from 11–25° N (green empty squares) and from 25–36° N (blue asterisks) on 3 and 9 August, without showing any significant separation from the extratropical observations.

started decreasing above ∼17 km (near cold point level), while for CH_3Cl, $CHCl_3$, and CH_2Br_2, strong altitude gradients in the mixing ratios started lower, near ∼14 km, and then decline steadily above that level, implying additional photochemical losses.

The mixing ratios of CFC-11, Halon-2402, and CCl_4 decreased by ∼7%, 18% and 12%, respectively at 19 km, the upper limit of the data, relative to the values at the base of the TTL, whereas CH_3Cl, $CHCl_3$, and CH_2Br_2 decreased by 15%, 63% and almost 85%, respectively . The difference is a measure of the difference in their photochemical lifetimes; for instance, the longer photochemical lifetime of CCl_4 relative to $CHCl_3$, and CH_2Br_2 (Clerbaux et al., 2007; Law et al., 2007). The influence of OH chemistry causes the concentrations of reactive species (with negligible photolysis rates) fall off quickly with altitude.

Figure 4 shows the comparison of in situ measurements for photolytic and OH-reactive species compared to results from the 1-D model, using photolysis rates alone in the photochemical loss terms of Eq. (2), coupled with CO_2-derived air transport rates (pink lines). The model agrees very well with the observed profiles for CFC-11, Halon-2402, and CCl_4 (Fig. 4a–c) consistent with their dominant chemical loss process being photolysis, mostly above the TTL. This result implies that the influence of older air from subtropics is small and/or well simulated in the 1-D framework, since these gases are severely depleted in old stratospheric air. Indeed, profiles for WAS species at subtropics (see data points binned by 11–25° N (green squares) and 25–36° N (blue asterisks) in Fig. 5d–f) were nearly identical with tropical data in TC4 (in contrast to CR-AVE). The comparisons of all 11 species are illustrated in Supplemental Fig. 1. Hence the model runs with w and K estimated using midlatitude CO_2 data, assuming small K and horizontal mixing with extratropics (see orange dashed lines in Fig. 5a–c) were indistinguishable from results of the 1-D model. These results support the application of our transport model to assess the processes that influence trace gas transport through the TTL, were indistinguishable from the $w-K$ model for the reactive tracers.

To simulate the observed profiles of the OH-reactive species, CH_3Cl, $CHCl_3$, and CH_2Br_2, we first used the monthly mean concentrations of OH in July derived from GMI run for 2007 (Considine et al., 2008) as shown in Fig. 5 (green dash-dot lines). This OH profile significantly improves the shape of the computed vertical profile, but the vertical gradient is not steep enough for any of the tracers. Horizontal mixing would have little effect, just as for

Table 1. Empirically derived OH concentrations with altitude (as shown in Fig. 6). Local chemical lifetimes listed have been averaged into 500-m intervals.

Alt	[OH]$\times 10^6$	Local Lifetime										
		CFC.11	Halon.2402	CCl_4	CH_3CCl_3	CH_3Cl	CH_3Br	$CHCl_3$	CH_2Br_2	$CHBr_3$	C_2Cl_4	Ethane
(km)	(molecule cm^{-3})	year						month			day	
14.5	2.5	116.3	15.9	37.6	8.7	2.4	2.7	6.3	4.6	19.7	49.5	48.6
15.0	2.5	89.4	13.1	29.2	8.4	2.6	2.8	6.7	4.9	19.8	50.2	50.1
15.5	2.4	57.8	9.5	19.2	7.9	2.9	2.9	7.3	5.2	19.8	51.5	52.6
16.0	2.3	38.1	7.0	12.8	7.0	3.2	3.0	8.1	5.7	19.7	52.8	55.3
16.5	2.2	25.4	5.2	8.5	6.1	3.6	2.9	8.8	6.0	19.5	53.9	57.6
17.0	2.1	17.5	4.0	5.9	5.0	3.7	2.7	9.2	6.1	18.9	54.9	58.6
17.5	1.9	12.3	3.1	4.1	4.1	3.6	2.3	9.1	6.0	18.1	55.8	58.1
18.0	1.8	8.8	2.4	3.0	3.3	3.6	2.0	9.2	5.9	17.2	57.0	58.3
18.5	1.6	6.3	1.8	2.1	2.7	3.7	1.7	9.6	5.9	16.1	58.5	59.2

the photolyzed tracers, discussed above, and convective inputs would tend to add more tracers, not less. We conclude that the results in Fig. 5a–c imply higher OH concentrations than given in the GMI model run. To determine OH concentrations that produce the best matches of the mixing ratio simulation to the observations, we multiplied the GMI OH profile by a scaling factor assumed to be a 2nd order polynomial function of altitude, and adjusted the 3 coefficients until a best fit was obtained. The resulting RMSEs between the optimal fits and the observations were 3% to 14%. We extensively tested different combinations of scaling profiles but did not find significantly different optimal profiles. Figure 5a–c show our optimal fits (in blue solid lines) for the species using the optimized 24-h mean OH profiles. The blue dashed lines represent the uncertainty range, corresponding to ±30% uncertainties in [OH] (denoted by blue dotted lines in Fig. 6), which have generally been considered as OH field-related error range in chemical transport models (Wang et al., 2008).

The empirically adjusted [OH] profile (blue solid line in Fig. 6) spans the range 1.6–2.7$\times 10^6$ molecule cm^{-3} between 14 km and 18.5 km, the top altitude of WAS data points. The average over the altitude range was 2.2±0.3$\times 10^6$ molecule cm^{-3} (±14% uncertainty) and the 500 m-bin average values are given in Table 1. For the purpose of testing the optimizing process, we repeated the same simulation with Geos-Chem-derived OH base profile (denoted by red dash-dot line in Fig. 6), yielding a nearly identical profile (in red solid line). Figure 6 also presents the actual vertical profiles of [OH] (not 24-h means) measured during the SPADE (Wennberg et al., 1995) and STRAT campaigns (Wennberg et al., 1998), for comparison. Our derived OH profile was consistent with the observations, lower than their high-sun values and higher than low-sun data, but slightly decreasing with altitude. Despite their dependence on the solar zenith angle (SZA), however, the observed OH concentrations do not seem to vary with altitude, as does our derived OH profile. To test the calculated OH profile, we computed model results and compared to in situ measurements for three different compounds, CH_3Br, CH_3CCl_3, and $CHBr_3$, spanning a range of photochemical lifetimes of a couple of weeks to a few years in the TTL. The data conformed closely to the model without further adjustment, as shown in Fig. 7, providing confidence in the OH concentrations derived from our model simulation. Note particularly the ∼0 values of $CHBr_3$ above ∼16 km. This result provides strong support for the framework using our $w-K$ 1-D formulation, versus a formulation relying on convective injection. If a major fraction of air at, say, 16.5 km, had been injected by convective storms, we would expect highly variable concentrations of this gas.

To derive an atomic Cl concentration in the TTL, we examined the profiles of two trace gases which are removed by reactions with both OH radicals and Cl atoms, but predominantly with Cl atoms: ethane and tetrachloroethene (C_2Cl_4). Both have rate constants for the reaction with Cl atoms 1000–2000 times higher than with OH radicals in the upper troposphere and TTL and neither has other significant sinks (e.g., Gupta et al., 1998; Rudolph et al., 1996). Figure 8 shows the model runs (represented by blue solid lines) for C_2Cl_4 and ethane performed using transport rates from our analysis of CO_2 data, reaction constants for OH reaction, and OH concentrations derived above from the analysis for CH_3Cl, $CHCl_3$, and CH_2Br_2. We note that the OH profile derived from the species that do not react rapidly with Cl gave a model result with excess concentrations of C_2Cl_4 and ethane in the middle and upper TTL. Addition of reactions with Cl atoms was first tested with the Cl atom profiles from the GMI model calculation (Considine et al., 2008) for July 2007, but loss rates were still insufficient to explain the measured profiles of C_2Cl_4 and ethane (see green dotted lines in Fig. 8). We then scaled the GMI Cl atom profile with a 1st order polynomial function with altitude to produce an optimal fit to the observations. The resulting Cl atom concentration profile, however, reveals some intrinsic features shown in the derived OH concentration profile like high Cl concentration near the bottom of the TTL and decreasing trend with altitude. These features seem less realistic for the atmospheric Cl distribution, suggesting cross–talk with errors

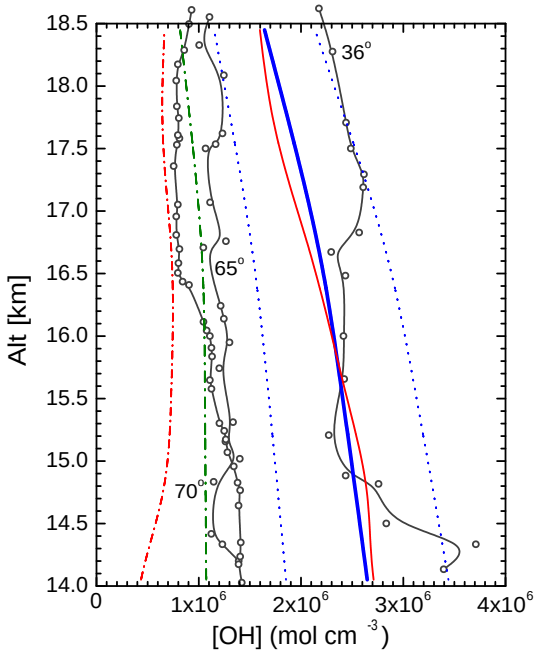

Fig. 6. Optimum OH concentrations to produce the best matches of the mixing ratio simulation to the observations are plotted against altitude, denoted by blue solid line. The base profile is the OH estimate from the GMI run (green dash-dotted line). The two blue dotted lines denote uncertainty range for ±30% of the [OH]. The optimization process was tested by repeating the analysis with the OH profile derived from Geos-Chem model run; base and resulting profiles are given in red dash-dotted line and red solid line, respectively. For comparison, the observed OH concentrations (Wennberg et al., 1995, 1998) are plotted as gray line and empty symbols, respectively. Shown is the solar zenith angle (SZA) of each observation profile.

from the OH-loss model. In order to obtain a more robust result, we derived a 24-h average Cl concentration for the altitude range between 14 km and 18.5 km instead of a profile by simulating the best fits to the measurements. The best-fit result was 2.4×10^3 atom cm^{-3}, which had uncertainty of $\pm0.6\times10^3$ atom cm^{-3} when the error propagated from the nominal uncertainty of ±30% of the estimated OH profile was considered. The derived Cl concentration is about two times larger than $1.3\pm1.0\times10^3$ atom cm^{-3}, the average of GMI-derived Cl concentrations, and is also more than 2–20 times larger than an average tropospheric chlorine concentration of the order of 0.1×10^3–1×10^3 atoms cm^{-3}, which was estimated using the budgets of ethane and C_2Cl_4 by Rudolph et al. (1996).

Finally, to examine whether our transport rates and OH radical and Cl atom concentrations which were empirically derived from the 5 August observations, are unambiguous for other flight data, we generated the vertical profiles for the chemical species stated above (shown in Fig. 9) by using their mixing ratios observed at the base of TTL on 6 August as the initial boundary values. Agreement between the data and the computed profiles with a set of input parameters determined above from the analysis on the 5 August data is reasonably good, capturing overall features of the observations, although the data set is more limited on this day.

4.3 Age spectra and chemical lifetimes for long- and short-lived species

The most often used time scale for atmospheric gases is the average global lifetime which is defined as the total burden of a compound divided by its globally, annually integrated loss rate. In steady state this burden divided by the lifetime is equal to the source emission needed to maintain current abundances. The global mean lifetime is thus useful for projecting the future mixing ratios (e.g., Clerbaux et al., 2007; Law et al., 2007).

However, it can not represent a fundamental time constant of the chemical system in the TTL and lower stratosphere, particularly for the gases with a range of local loss frequencies, such as photodissociation of halogenated compounds. The local loss frequencies correspond to spatial and temporal variations in the reactive radical concentration (e.g., OH, $O(^1D)$, and Cl) and solar flux in both regions. Hence, in order to estimate the contribution of the tropospheric source gases to stratospheric chlorine/bromine loading and thus to evaluate model schemes for stratospheric chemistry, a local chemical lifetime should be considered and determined at the primary entry point for the stratosphere. The local lifetimes are defined as $(\tau)^{-1} = (\tau_{OH})^{-1} + (\tau_J)^{-1}$ where τ_{OH} and τ_J are the lifetimes due to reactions with OH and photolysis, respectively. (Note for ethane and C_2Cl_4 in our analysis, $(\tau)^{-1} = (\tau_{OH})^{-1} + (\tau_{Cl})^{-1}$, where τ_{Cl} is the lifetime due to reactions with Cl atoms). We estimated the local lifetimes for the species examined above using the derived vertical profiles of OH radicals and Cl atoms and altitude-varying photolysis rates. The calculated chemical lifetimes of 500-m bin average around 18 km, approximately equivalent to the top boundary of the TTL are 8.8, 2.4, 3.0, 3.3, 3.6, 2.0 years, 9.2, 6.0 months, and 17.2 days for CFC-11, Halon-2402, CCl_4, CH_3CCl_3, CH_3Cl, CH_3Br, $CHCl_3$, CH_2Br_2, and $CHBr_3$, respectively. The results for other altitudes are given in Table 1. We note that the estimated local lifetimes at the 18 km level for the long-lived species, of which the main loss process is photolysis in the stratosphere, such as CFC-11, Halon-2402, CCl_4, and CH_3CCl_3 are significantly reduced by 40–90% compared with the global mean lifetimes provided in WMO report due most likely to geographic proximity to their sink region. Most importantly, for the relatively short-lived species destroyed dominantly by reaction with OH radicals, such as CH_3Cl, CH_3Br, $CHCl_3$, and CH_2Br_2 the local lifetimes are 1.5–4 times longer than the average global lifetimes. This is due to the fact that extremely low temperatures in the TTL and the lower stratosphere slow down the reaction of OH with these compounds. These results imply

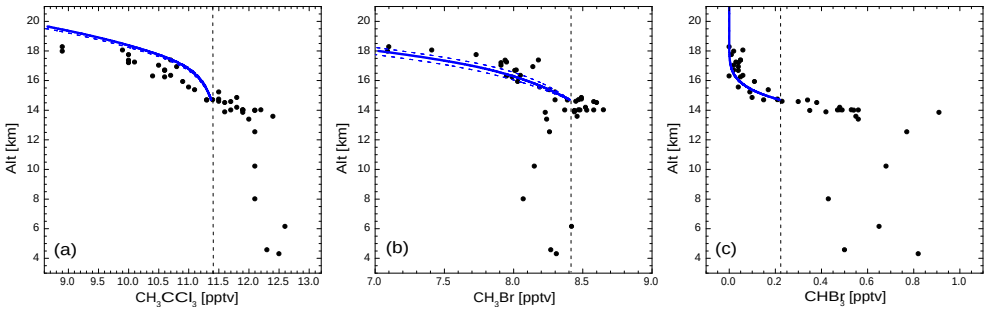

Fig. 7. Vertical distributions of **(a)** CH_3CCl_3, **(b)** CH_3Br, and **(c)** $CHBr_3$. Symbols are the same as in Fig. 5. The blue dotted lines denote the fits with ±30% uncertainties in [OH].

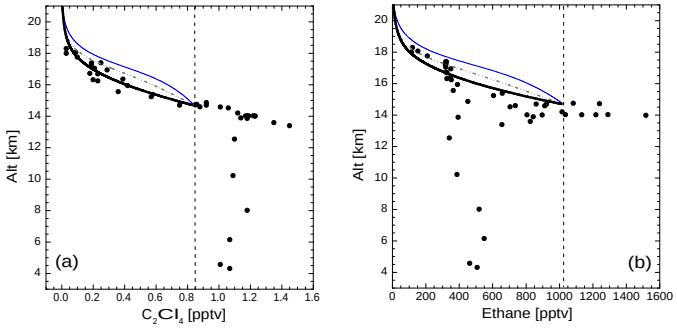

Fig. 8. Vertical distributions of **(a)** C_2Cl_4 and **(b)** ethane. The 1-D model results using the optimum OH profile shown in Fig. 6 (blue solid lines) overestimate the observations denoted by black solid circles. The difference between the simulation and observation should correspond to the reaction with Cl atoms, but the GMI-derived Cl atoms are not sufficient (gray dotted lines). The best matches are generated by adjusting 24-h average value for Cl concentrations between 14 km and 18.5 km and are represented by black solid lines.

that these gases have a greater probability to reach the stratosphere through the TTL than might be expected based on their global lifetimes.

Figure 10a shows the age spectra for both non-reactive (CO_2) and reactive species at different altitudes in both TC4 and CR-AVE, and Fig. 10b shows the associated vertical profiles of fraction remaining in the atmosphere, as for gases of various mean lifetimes. The age spectra are sharper, and the transit times shorter, for CR-AVE as compared to TC4. During CR-AVE, air entering the stratosphere would have more than 20% of the boundary layer concentration of a halogen precursor whose lifetime longer than 30 days, and more than 60% would survive transit of the TTL if the lifetime exceeded 60 days. Even during TC4, more than 20% of the input concentration would survive for gases with lifetimes >60 days.

Model studies for the midlatitude ozone depletion have indicated that the contributions of short-lived compounds transported as both organic source gases and inorganic product gases to the stratospheric inorganic halogens may be more significant than those of the long-lived species in the lowermost stratosphere (e.g., Dvortsov et al., 1999; Ko et al., 2003; Salawitch et al., 2005; Sinnhuber et al., 2009). Here, the species $CHCl_3$, CH_2Cl_2, CH_2Br_2, and $CHBr_3$, are in general classified as the "very short-lived species" (with atmospheric lifetimes of less than 6 months); $CHCl_3$ and CH_2Cl_2 contribute the most very short-lived organic chlorine (20 and 40 ppt Cl, respectively) to both the marine boundary layer and the upper troposphere. Similarly, CH_2Br_2, and $CHBr_3$ represent more than 80% of the very short-lived organic bromine in both regions, accounting for 3–4 ppt of Br. Our estimates of the local lifetimes near 18-km altitude in the TTL for $CHCl_3$, CH_2Cl_2, CH_2Br_2, and $CHBr_3$ were 9.2, 8.5, and 6.0 months, and 17.2 days, indicating that all of these can contribute their halogen payload to the stratosphere, possibly excepting $CHBr_3$. An important implication of these results is that the organic chlorine and bromine in "very short-lived source gases" could reach the stratosphere even before chemical breakdown to product gases, and their delivery into the stratosphere through the TTL does not require the rare deep convection events directly to levels above 380 K, but instead can occur via vertical advection through the TTL.

Salawitch et al. (2005) noticed from the data shown in Wamsley et al. (1998) the difference between bromine delivered to the stratosphere by "long-lived" source gases, and estimates of total stratospheric bromine derived from observations of bromine monoxide (BrO) (denoted "additional" stratospheric bromine in WMO report; Law et al., 2007), and suggested additional bromine supply of 4–8 ppt near the

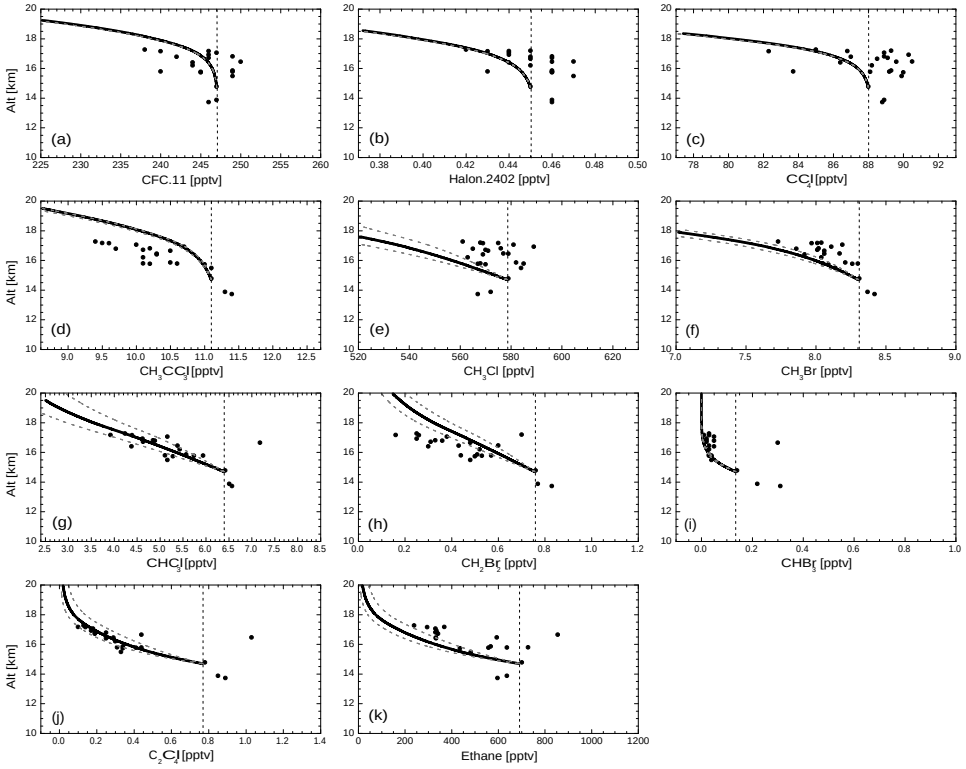

Fig. 9. Vertical distributions of **(a)** CFC-11, **(b)** Halon-2402, **(c)** CCl_4, **(d)** CH_3CCl_3, **(e)** CH_3Cl, **(f)** CH_3Br, **(g)** $CHCl_3$, **(h)** CH_2Br_2, **(i)** $CHBr_3$, **(j)** C_2Cl_4 and **(k)** ethane. Plotted are individual data points (solid circles) measured by WAS on 6 August and the 1-D model results (solid lines) with a set of input parameters determined from the analysis on the 5 August data.

tropopause, which was confirmed with ∼5 ppt derived from recent BrO observations (Dorf et al., 2008). Our observations of CH_2Br_2 and $CHBr_3$ near the tropopause (cold point level; ∼17 km) reveal that ∼0.7 ppt and ∼0.1 ppt bromine can be carried into the stratosphere across the tropopause in CH_2Br_2 and $CHBr_3$ forms, respectively. If we assume that within the TTL inorganic bromine decomposed from the species were not removed, due to suppressed convection above the 360-K level (i.e., the base of the TTL) and thus inefficient scavenging by falling ice, all the bromine released within the TTL might reach the stratosphere (e.g., Sinnhuber and Folkins, 2006). Then the organic bromine abundance of ∼2.3 ppt observed at $\theta = \sim 360$ K in the VSL species could be contributed by vertical ascent through the TTL as the source gases plus inorganic product gases. The abundance gradients for organic Br between the base and top of the TTL (∼1.5 ppt bromine) would in this case correspond to injection of product gases generated within the TTL; the relative contribution of source gas injection vs. inorganic product gas injection would be ∼40% vs. ∼60%.

The same analysis performed for $CHCl_3$ and CH_2Cl_2 showed that ∼54 ppt chlorine can reach stratosphere as the VLS source gases, but the maximum chlorine injection of inorganic product gases would be only ∼6 ppt, ∼10% of the total chlorine contribution via vertical ascent through the TTL.

Our data for the bromine species, and the analysis, are compatible with early aircraft observations (Schauffler et al., 1999), recent balloon-borne measurements (Laube et al., 2008) and recent model studies (Gettelman et al., 2009; Aschmann et al., 2009; Hossaini et al., 2010; Liang et al., 2010), which infer a contribution of CH_2Br_2 and $CHBr_3$ in the range of ∼2–5 ppt. Our estimate of about 2.3 ppt bromine contribution from CH_2Br_2 and $CHBr_3$ through the TTL explains just half of "additional" stratospheric bromine derived from BrO measurements. The discrepancy is more likely due to existence of unknown source gases (e.g., Laube et al., 2008) and high variability of the tropospheric VSL species in time and space (e.g., Quack and Wallace, 2003; Laube et al., 2008; Liang et al., 2010).

5 Conclusions

This study has investigated the distributions and lifetimes of radiatively and chemically important long- and short-lived reactive species in the TTL and lower stratosphere, using empirical air mass transport rates characterized by CO_2 data and empirically derived profiles of radical concentrations from a set of tracers with a large span of photochemical lifetimes. We have derived altitude-dependent ascent rate profiles and

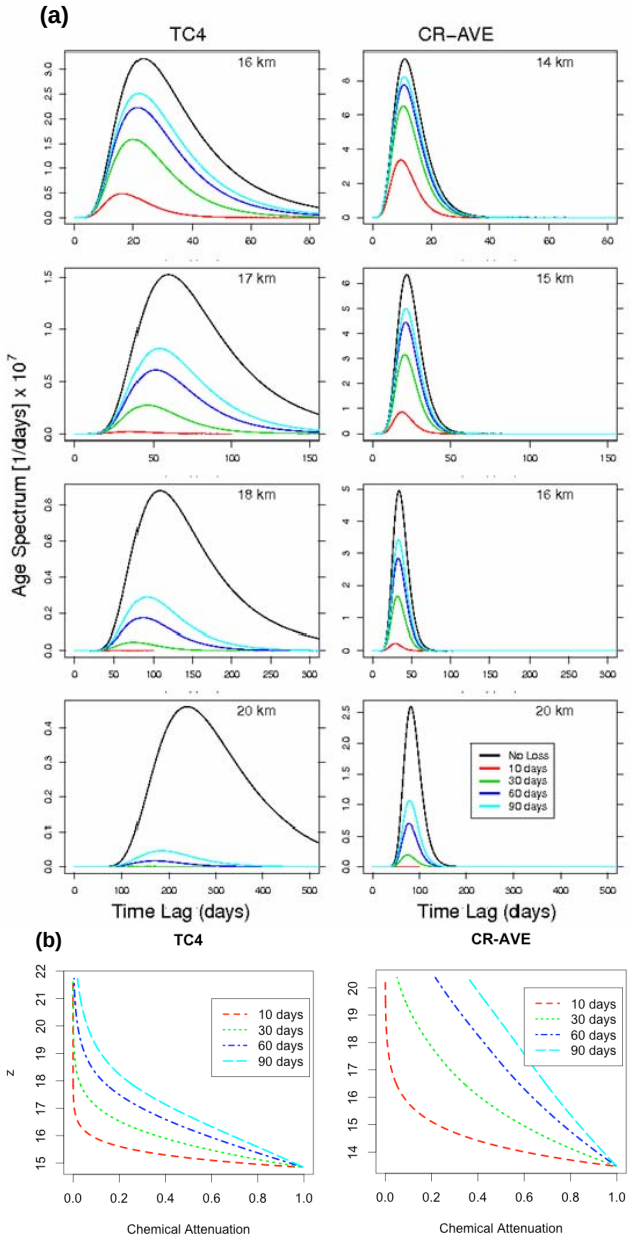

Fig. 10. **(a)** Age spectra for species with different lifetimes, in Northern summer (TC4) and winter (CR-AVE). **(b)** Surviving fraction of gases transiting the TTL, plotted versus altitude, for different lifetimes within the TTL.

a mean diffusion coefficient for the TTL and lower stratosphere from in situ observations of CO_2 mixing ratios, collected during the TC4 campaign in August 2007 and the CR-AVE campaign in January 2006, aboard the NASA WB-57F aircraft. The derived air transport properties in combination with well-defined photochemical loss processes can represent net transport and photochemical loss of the reactive species. Precise measurements of organic chlorine and bromine containing compounds from whole air samples were used to constrain the chemical parameters for the TTL and tropical lower stratosphere, i.e., the 24-h mean altitude profile of OH radical and 24-h average of atomic Cl concentration for the altitude range between 14 km and 18.5 km. The observed altitude profiles of the species examined here, together with the determined transport and chemical conditions for our model, were shown to accurately simulate the local photochemical lifetimes.

The empirically-derived vertical distributions of OH radical and atomic Cl concentrations in the TTL and lower stratosphere should provide new tests of model inputs for photochemical model calculations in the regions, of which the unique dynamical and chemical properties have not, to date, been addressed well in most models. Although OH concentrations were ∼2 times higher than computed by models, the inferred local chemical lifetimes of long- and short-lived species were significantly longer than corresponding mean global lifetimes. Our analysis indicates that very short-lived species such as $CHCl_3$, CH_2Cl_2, and CH_2Br_2 can readily reach the stratosphere via large-scale slow ascent though the TTL even under normal dynamic conditions (i.e., not solely in deep convective events that enter the stratosphere directly), confirming contributions of the chlorine- and bromine-containing very short-lived organic source gases to stratospheric chlorine and/or bromine loading.

In view of the importance of air transport mechanisms on the stratospheric loading, the uncertainties in the role of short-lived halogen precursors need to be addressed, with particular attention to observations that define the role of quasi-horizontal mixing with the extratropics and convective inputs into the TTL or the midlatitude stratosphere. The present analysis has been focused on just one period in August 2007. Systematic tracer measurements over a period of years, covering more of the seasonal cycle, are needed to investigate seasonal variations in the derived parameters above and eventually to help predict impacts of halogens originated from the surface on future column ozone depletion. Additionally the tropospheric distributions of the short-lived chemical species are highly variable in time and space due to the short lifetimes, which leads to the uncertainty in the input values at the base of the TTL.

Even with these limitations, this study demonstrates that in situ, high resolution measurements of CO_2 and long-/short-lived chemical species provide unique signals for defining air transport rates and chemical conditions governing the distributions of the chemical compounds in the TTL and lower stratosphere, and it is clear that short-lived precursor gases survive transit of the TTL to enter the stratosphere in the tropics.

Supplementary material related to this article is available online at: http://www.atmos-chem-phys.net/10/6669/2010/acp-10-6669-2010-supplement.pdf.

Acknowledgements. We thank the NASA WB-57F pilots and crews for the dedicated efforts. This work was supported by NASA grants NNG05GN82G, NNX07AK98G, and NNX07AL10G to Harvard University and NASA grants NNG05GGN80G and NNX09AJ25G to the University of Miami. We thank R. Lueb for valuable support in the deployment of the Whole Air Sampler, Xiaorong Zhu and Leslie Pope for technical support in the UM laboratory, and Jennifer Logan and Inna Megretskaia for providing us with the GMI data and helpful discussion.

Edited by: W. T. Sturges

References

Andrews, A. E., Boering, K. A., Daube, B. C., Wofsy, S. C., Hintsa, E. J., Weinstock, E. M., and Bui, T. P.: Empirical age spectra for the lower tropical stratosphere from in situ observations of CO_2: Implications for stratospheric transport, J. Geophys. Res., 104(D21), 26581–26596, 1999.

Andrews, A. E., Boering, K. A., Daube, B. C., Wofsy, S. C., Loewenstein, M., Jost, H., Podolske, J. R., Webster, C. R., Herman, R. L., Scott, D. C., Flesch, G. J., Moyer, E. J., Elkins, J. W., Dutton, G. S., Hurst, D. F., Moore, F. L., Ray, E. A., Romashkin, P. A., and Strahan, S. E.: Mean ages of stratospheric air derived from in situ observations of CO_2, CH_4, and N_2O, J. Geophys. Res., 106(D23), 32295–32314, 2001a.

Andrews, A. E., Boering, K. A., Wofsy, S. C., Daube, B. C., Jones, D. B., Alex, S., Loewenstein, M., Podolske, J. R., and Strahan, S. E.: Empirical age spectra for the midlatitude lower stratosphere from in situ observations of CO_2: Quantitative evidence for a subtropical "barrier" to horizontal transport, J. Geophys. Res., 106(D10), 10257–10274, 2001b.

Aschmann, J., Sinnhuber, B.-M., Atlas, E. L., and Schauffler, S. M.: Modeling the transport of very short-lived substances into the tropical upper troposphere and lower stratosphere, Atmos. Chem. Phys., 9, 9237–9247, doi:10.5194/acp-9-9237-2009, 2009.

Boering, K. A., Dessler, A. E., Loewenstein, M., McCormick, M. P., Podolske, J. R., Weinstock, E. M., and Yue, G. K.: Measurements of stratospheric carbon dioxide and water vapor at northern midlatitudes: Implications for troposphere-to-stratosphere transport, Geophys. Res. Lett., 22(20), 2737–2740, 1995.

Boering, K. A., Wofsy, S. C., Daube, B. C., Schneider, H. R., Loewenstein, M., and Podolske, J. R.: Stratospheric mean ages and transport rates from observations of carbon dioxide and nitrous oxide, Science, 274(5291), 1340–1343, 1996.

Clerbaux, C., Cunnold, D. M., Anderson, J., Engel, A., Fraser, P. J., Mahieu, E., Manning, A., Miller, J., Montzka, S. A., Nassar, R., Prinn, R., Reimann, S., Rinsland, C. P., Simmonds, P., Verdonik, D., Weiss, R., Wuebbles, D., and Yokouchi, Y.: Long-Lived Compounds, Chapter 1 in Scientific Assessment of Ozone Depletion: 2006, Global Ozone Research and Monitoring Project, World Meteorological Organization, Geneva, Switzerland, Report No. 50, 572 pp., 2007.

Considine, D. B., Logan, J. A., and Olsen, M. A.: Evaluation of near-tropopause ozone distributions in the Global Modeling Initiative combined stratosphere/troposphere model with ozonesonde data, Atmos. Chem. Phys., 8(9), 2365–2385, doi:10.5194/acp-9-9237-2009, 2008.

Conway, T. J., Tans, P. P., Waterman, L. S., and Thoning, K. W.: Evidence for interannual variability of the carbon cycle from the National Oceanic and Atmospheric Administration/ Climate Monitoring and Diagnostics Laboratory global air sampling network, J. Geophys. Res., 99(D11), 22831–22855, 1994.

Daube, B. C., Boering, K. A., Andrews, A. E., and Wofsy, S. C.: A high-precision fast-response airborne CO_2 analyzer for in situ sampling from the surface to the middle stratosphere, J. Atmos. Oceanic Technol., 19(10), 1532–1543, 2002.

Dorf, M., Butz, A., Camy-Peyret, C., Chipperfield, M. P., Kritten, L., and Pfeilsticker, K.: Bromine in the tropical troposphere and stratosphere as derived from balloon-borne BrO observations, Atmos. Chem. Phys., 8, 7265–7271, doi:10.5194/acp-8-7265-2008, 2008.

Dvortsov, V. L., Geller, M. A., Solomon, S., Schauffler, S. M., Atlas, E. L., and Blake, D. R.: Rethinking reactive halogen budgets in the midlatitude lower stratosphere, Geophys. Res. Lett., 26(12), 1699–1702, doi:10.1029/1999GL900309, 1999.

Flocke, F., Herman, R. L., Salawitch, R. J., Atlas, E., Webster, C. R., Schauffler, S. M., Lueb, R. A., May, R. D., Moyer, E. J., Rosenlof, K. H., Scott, D. C., Blake, D. R., and Bui, T. P.: An examination of chemistry and transport processes in the tropical lower stratosphere using observations of long-lived and short-lived compounds obtained during STRAT and POLARIS, J. Geophys. Res., 104(D21), 26625–26642, 1999.

Fueglistaler, S., Dessler, A. E., Dunkerton, T. J., Folkins, I., Fu, Q., and Mote, P. W.: Tropical Tropopause Layer, Rev. Geophys., 47, RG1004, doi:1010.1029/2008RG000267, 2009.

Gettelman, A. and Forster, P. M. d. F.: A climatology of the tropical tropopause layer, J. Meteorol. Soc. Jpn., 80, 911–924, 2002.

Gettelman, A., Lauritzen, P. H., Park, M., and Kay, J. E.: Processes regulating short-lived species in the tropical tropopause layer, J. Geophys. Res., 114, D13303, doi:10.1029/2009JD011785, 2009.

Gupta, M. L., Cicerone, R. J., Blake, D. R., Rowland, F. S., and Isaksen, I. S. A.: Global atmospheric distributions and source strengths of light hydrocarbons and tetrachloroethene, J. Geophys. Res., 103(D21), 28219–28235, 1998.

Hall, T. M. and Waugh, D. W.: Timescales for stratospheric circulation derived from tracers, J. Geophys. Res. 102(D7), 8991–9001, 1997.

Hall, T. M. and Waugh, D. W.: Stratospheric residence time and its relationship to mean age, J. Geophys. Res. 105(D5), 6773–6782, 2000.

Hossaini, R., Chipperfield, M. P., Monge-Sanz, B. M., Richards, N. A. D., Atlas, E., and Blake, D. R.: Bromoform and dibromomethane in the tropics: a 3-D model study of chemistry and transport, Atmos. Chem. Phys., 10, 719–735, doi:10.5194/acp-10-719-2010, 2010.

Ko, M. K. W., Poulet, G., Blake, D. R., et al.: Very short-lived halogen and sulfurubstances, Scientific assessment of ozone depletion: 2002, Global Ozone Research and Monitoring Project. Report No. 47, Chapter 2, World Meteorological Organization, Geneva, 2003.

Kruger, K., Tegtmeier, S., and Rex, M.: Variability of residence

time in the Tropical Tropopause Layer during Northern Hemisphere winter, Atmos. Chem. Phys., 9, 6717–6725, 2009, http://www.atmos-chem-phys.net/9/6717/2009/.

Law, K. S., Sturges, W. T., Blake, D. R., Blake, N. J., Burkholder, J. B., Butler, J. H., Cox, R. A., Haynes, P. H., Ko, M. K. W., Kreher, K., Mari, C., Pfeilsticker, K., Plane, J. M. C., Salawitch, R. J., Schiller, C., Sinnhuber, B.-M., Glasow, R. v., Warwick, N. J., Wuebbles, D. J., and Yvon-Lewis, S. A.: Halogenated Very Short-Lived Substances, Chapter 2 in Scientific Assessment of Ozone Depletion: 2006, Global Ozone Research and Monitoring Project, World Meteorological Organization, Geneva, Switzerland, Report No. 50, 572 pp., 2007.

Levine, J. G., Braesicke, P., Harris, N. R. P., Savage, N. H., and Pyle, J. A.: Pathways and timescales for troposphere-to-stratosphere transport via the tropical tropopause layer and their relevance for very short lived substances, J. Geophys. Res., 112, D04308, doi:04310.01029/02005JD006940, 2007.

Liang, Q., Stolarski, R. S., Kawa, S. R., Nielsen, J. E., Douglass, A. R., Rodriguez, J. M., Blake, D. R., Atlas, E. L., and Ott, L. E.: Finding the missing stratospheric Br_y: a global modeling study of $CHBr_3$ and CH_2Br_2, Atmos. Chem. Phys., 10, 2269–2286, doi:10.5194/acp-10-2269-2010, 2010.

McLinden, C. A., Olsen, S. C., Hannegan, B., Wild, O., and Prather, M. J.: Stratospheric ozone in 3-D models: A simple chemistry and the cross-tropopause flux, J. Geophys. Res., 105(D11), 14653–14665, 2000.

Neu, J. L. and Plumb, R. A.: Age of air in a "leaky pipe" model of stratospheric transport, J. Geophys. Res., 104(D16), 19,243–19,256, 1999.

Park, S., Jimenez, R., Daube, B. C., Pfister, L., Conway, T. J., Gottlieb, E. W., Chow, V. Y., Curran, D. J., Matross, D. M., Bright, A., Atlas, E. L., Bui, T. P., Gao, R.-S., Twohy, C. H., and Wofsy, S. C.: The CO_2 tracer clock for the Tropical Tropopause Layer, Atmos. Chem. Phys., 7(14), 3989–4000, doi:10.5194/acp-7-3989-2007, 2007.

Parrington, M., Jones, D. B. A., Bowman, K. W., Horowitz, L. W., Thompson, A. M., Tarasick, D. W., and Witte, J. C.: Estimating the summertime tropospheric ozone distribution over North America through assimilation of observations from the Tropospheric Emission Spectrometer, J. Geophys. Res., 113, D18307, doi:18310.11029/12007JD009341, 2008.

Pfister, L., Selkirk, H. B., Jensen, E. J., Schoeberl, M. R., Toon, O. B., Browell, E. V., Grant, W. B., Gary, B., Mahoney, M. J., Bui, T. V., and Hintsa, E.: Aircraft observations of thin cirrus clouds near the tropical tropopause, J. Geophys. Res., 106(D9), 9765–9786, 2001.

Pfister, L., Selkirk, H. B., Starr, D. O., Rosenlof, K., and Newman, P. A.: A Meteorological Overview of the TC4 Mission, J. Geophys. Res., doi:10.1029/2009JD013316, in press, 2010.

Ploeger, F., Konopka, P., Gunther, G., Grooß, J.-U., and Muller, R.: Impact of the vertical velocity scheme on modeling transport in the tropical tropopause layer, J. Geophys. Res., 115, D03301, doi:10.1029/2009JD012023, 2010.

Plumb, R. A.: A "tropical pipe" model of stratospheric transport, J. Geophys. Res., 101(D2), 3957–3972, 1996.

Proffitt, M. H. and McLaughlin, R. L.: Fast-response dual-beam UV-absorption ozone photometer suitable for use on stratospheric balloons, Rev. Sci. Instrum., 54(12), 1719–1728, 1983.

Quack, B. and Wallace, D. W. R.: Air-sea flux of bromoform: Controls, rates, and implications, Global Biogeochem. Cy., 17(1), 1023, doi:10.1029/2002GB001890, 2003.

Rudolph, J., Koppmann, R., and PlassDulmer, C.: The budgets of ethane and tetrachloroethene: Is there evidence for an impact of reactions with chlorine atoms in the troposphere?, Atmos. Environ., 30(10-11), 1887–1894, 1996.

Salawitch, R. J., Wofsy, S. C., Wennberg, P. O., Cohen, R. C., Anderson, J. G., Fahey, D. W., Gao, R. S., Keim, E. R., Woodbridge, E. L., Stimpfle, R. M., Koplow, J. P., Kohn, D. W., Webster, C. R., May, R. D., Pfister, L., Gottlieb, E. W., Michelsen, H. A., Yue, G. K., Prather, M. J., Wilson, J. C., Brock, C. A., Jonsson, H. H., Dye, J. E., Baumgardner, D., Proffitt, M. H., Loewenstein, M., Podolske, J. R., Elkins, J. W., Dutton, G. S., Hintsa, E. J., Dessler, A. E., Weinstock, E. M., Kelly, K. K., Boering, K. A., Daube, B. C., Chan, K. R., and Bowen, S. W.: The diurnal-variation of hydrogen, nitrogen, and chlorine radicals: Implications for the heterogeneous production of HNO_2, Geophys. Res. Lett., 21(23), 2551–2554, 1994.

Salawitch, R. J., Weisenstein, D. K., Kovalenko, L. J., Sioris, C. E., Wennberg, P. O., Chance, K., Ko, M. K. W., and McLinden, C. A.: Sensitivity of ozone to bromine in the lower stratosphere, Geophys. Res. Lett., 32, L05811, doi:10.1029/2004GL021504, 2005.

Sander, S. P., Friedl, R. R., Ravishankara, A. R., Golden, D. M., Kolb, C. E., Kurylo, M. J., Molina, M. J., Moortgat, G. K., Finlayson-Pitts, B. J., Wine, P. H., Huie, R. E., and Orkin, V. L.: Chemical kinetics and photochemical data for use in atmospheric studies evaluation No. 15, Jet Propul. Lab., Pasadena, California, USA, 2006.

Schauffler, S. M., Atlas, E. L., Blake, D. R., Flocke, F., Lueb, R. A., Lee-Taylor, J. M., Stroud, V., and Travnicek, W.: Distributions of brominated organic compounds in the troposphere and lower stratosphere, J. Geophys. Res., 104(D17), 21513–21535, 1999.

Schauffler, S. M., Atlas, E. L., Donnelly, S. G., Andrews, A., Montzka, S. A., Elkins, J. W., Hurst, D. F., Romashkin, P. A., Dutton, G. S., and Stroud, V.: Chlorine budget and partitioning during the Stratospheric Aerosol and Gas Experiment (SAGE) III Ozone Loss and Validation Experiment (SOLVE), J. Geophys. Res., 108(D5), 4173, doi:4110.1029/2001JD002040, 2003.

Schneider, H. R., D. B. A. Jones, G.-Y. Shi, and M. B. McElroy, Analysis of the residual mean transport in the stratosphere. Part I: Model description and comparison with satellite data, J. Geophys. Res., 105(D15), 19,991-20,011, 2000.

Schoeberl, M. R., Douglass, A. R., Stolarski, R. S., Pawson, S., Strahan, S. E., and Read, W.: Comparison of lower stratospheric tropical mean vertical velocities, J. Geophys. Res., 113, D24109, doi:24110.21029/22008JD010221, 2008.

Scott, S. G., Bui, T. P., Chan, K. R., and Bowen, S. W.: The meteorological measurement system on the NASA ER-2 aircraft J. Atmos. Ocean. Technol., 7(4), 525–540, 1990.

Sinnhuber, B.-M. and Folkins, I.: Estimating the contribution of bromoform to stratospheric bromine and its relation to dehydration in the tropical tropopause layer, Atmos. Chem. Phys., 6, 4755–4761, 2006, http://www.atmos-chem-phys.net/6/4755/2006/.

Sinnhuber, B.-M., Sheode, N., Sinnhuber, M., Chipperfield, M. P., and Feng, W.: The contribution of anthropogenic bromine emissions to past stratospheric ozone trends: a modelling study, Atmos. Chem. Phys., 9(8), 2863–2871, doi:10.5194/acp-9-2863-

2009, 2009.

Toon, O. B., Starr, D. O., Jensen, E. J., Newman, P. A., Platnick, S. E., Schoeberl, M. R., Wennberg, P. O., Wofsy, S. C., Kurylo, M. J., Maring, H., Jucks, K. W., Craig, M. S., Vasques, M. F., Pfister, L., Rosenlof, K., Selkirk, H. B., Colarco, P. R., Kawa, S. R., Mace, G. G., Minnis, P., and Pickering, K. E.: Planning and Implementation of the Tropical Composition, Cloud and Climate Coupling Experiment (TC4), J. Geophys. Res., 115, D00J04, doi:10.1029/2009JD013073, 2010.

Wamsley, P. R., Elkins, J. W., Fahey, D. W., et al.: Distribution of halon-1211 in the upper troposphere and lower stratosphere and the 1994 total bromine budget, J. Geophys. Res., 103(D1), 1513–1526, 1998.

Wang, S., Pickett, H. M., Pongetti, T. J., Cheung, R., Yung, Y. L., Shim, C., Li, T. C. Q., Salawitch, R. J., Jucks, K. W., Drouin, B., and Sander, S. P.: Validation of Aura Microwave Limb Sounder OH measurements with Fourier Transform Ultra-Violet Spectrometer total OH column measurements at Table Mountain, California, J. Geophys. Res., 113, D22301, doi:22310.21029/22008JD009883, 2008.

Wennberg, P. O., Hanisco, T. F., Cohen, R. C., Stimpfle, R. M., Lapson, L. B. J., and Anderson, J. G.: In-situ measurements of OH and HO_2 in the upper troposphere and stratosphere, J. Atmos. Sci., 52(19), 3413–3420, 1995.

Wennberg, P. O., Hanisco, T. F., Jaegle, L., Jacob, D. J., Hintsa, E. J., Lanzendorf, E. J., Anderson, J. G., Gao, R.-S., Keim, E. R., Donnelly, S. G., Negro, L. A. D., Fahey, D. W., McKeen, S. A., Salawitch, R. J., Webster, C. R., May, R. D., Herman, R. L., Proffitt, M. H., Margitan, J. J., Atlas, E. L., Schauffler, S. M., Flocke, F., McElroy, C. T., and Bui, T. P.: Hydrogen radicals, nitrogen radicals, and the production of O_3 in the upper troposphere, Science, 279(5347), 49–53, 1998.